A semi-empirical model for ship speed loss prediction at head sea and its validation by full-scale measurements

Ocean Engineering 209 (2020) 107494

Contents lists available at ScienceDirect

Ocean Engineering

journal homepage: www.elsevier.com/locate/oceaneng

A semi-empirical model for ship speed loss prediction at head sea and its validation by full-scale measurements

Xiao Lang *, Wengang Mao

Department of Mechanics and Maritime Sciences, Division of Marine Technology, Chalmers University of Technology, SE-412 96, Gothenburg, Sweden

ARTICLE INFO

Keywords:
Speed loss
Irregular sea
Head wave
Added resistance due to waves
Full-scale measurements

ABSTRACT

This paper proposes a semi-empirical model to estimate a ship's speed loss at head sea. In the model, the formulas to estimate a ship's added resistance due to waves have been further developed to better consider the ship hull forms, in addition to other main particulars. Based on the model experimental tests of 11 ships in regular head waves, the new formulas have more flexible forms and can better fit the test results than other similar models. In addition, this model proposes a significant wave height based correction factor multiplied to the conventional integration to compute wave resistance in irregular waves. This factor is supposed to consider the impact of coupled ship motions in high waves on a ship's added resistance due to waves. The model is validated by the full-scale measurement from two vessels, a PCTC and a chemical tanker. The encountered weather conditions along the sailing routes are extracted from the reanalysis metocean data. The results indicate that the proposed model can provide quite accurate predictions of ship speed loss in head sea operations.

1. Introduction

The enhancement of several maritime regulations, such as the Energy Efficiency Design Index (EEDI) and Energy Efficiency Operational Indicator (EEOI), is promoting the development of energy efficiency measures to reduce fuel consumption and greenhouse gas emissions (IMO, 2014, 2009). The EEDI and EEOI emphasize the importance of considering a ship's energy performance in her actual sailing environments, where involuntary ship speed losses are expected in adverse sea conditions (Prpić-Oršić and Faltinsen, 2012; Brandsæter and Vanem, 2018; Lu et al., 2015). A reliable method to describe a ship's speed loss at such environments is often required for both ship design and operations to increase a ship's energy efficiency (Wang et al., 2019; DNV-GL, 2015). For a ship sailing under a certain sea condition at a specific engine power, the speed loss ΔV is defined as the involuntary reduction between the ship speed in calm sea condition V_{calm}, and the real speed V_{real} under the sea environment as:

$$\Delta V = V_{calm} - V_{real} \tag{1}$$

where the speed loss is mainly caused by the added resistance due to wave and wind (Pérez Arribas, 2007). Normally, a ship's total resistance that should be overcome by ship propulsion to push a ship forward is divided into calm water resistance, added resistance due to wind and waves, and other small effects (ISO, 2015). The calm water resistance and added resistance due to wind are relatively easy to be estimated by model tests or some well-developed semi-empirical formulas (Holtrop and Mennen, 1982), but the accurate estimation of the added resistance due to waves is challenging, and it is an essential part for a ship's speed loss prediction.

Three energy components transmitted to the surrounding water are commonly related to the added resistance in waves. The first component is the diffraction induced resistance when incident wave reflecting on the ship hull, dominating for short waves. The second component is the drift force from radiated waves, produced by the ship motions in the long wave region. The third component is connected viscous effect and is always neglected since the viscous damping is minor compared to the hydrodynamic damping of ship motions. Thus, the added resistance due to waves could be simplified as a non-viscous phenomenon, and make it possible to scale the resistance from model test to full-scale estimation (Strom-Tejsen et al., 1973). In addition, some numerical methods are available to estimate the added resistance due to waves. Except for the computation expensive Computational Fluid Dynamics (CFD) methods, there are several numerical approaches based on slender-body theory or 3D panel method (ITTC, 2018). The development of various methods to estimate added resistance due to waves is briefly summarized in Fig. 1.

Havelock (1942) first attempted to calculate the added resistance with the integration of the longitudinal pressure forces over the wetted

* Corresponding author.
E-mail address: xiao.lang@chalmers.se (X. Lang).

https://doi.org/10.1016/j.oceaneng.2020.107494
Received 4 February 2020; Received in revised form 27 April 2020; Accepted 4 May 2020
Available online 22 May 2020

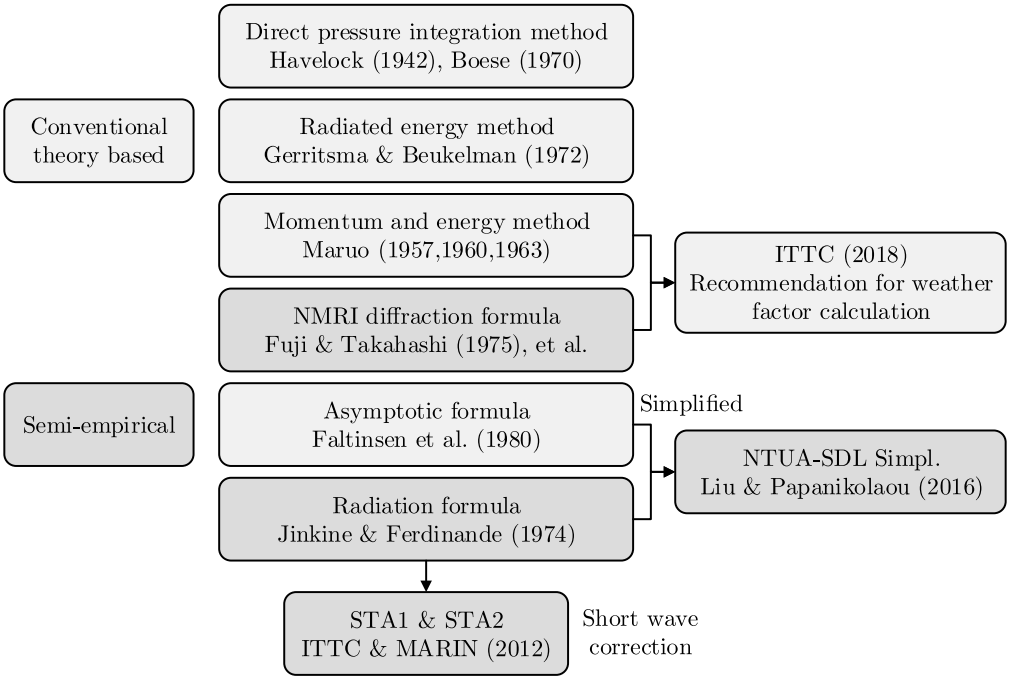

Fig. 1. Brief summary of the development of various methods to estimate wave induced added resistance.

ship hull. In 1970, Boese (1970) continued Havelock's work via using strip theory, named as the direct pressure integration method. Maruo (1957) proposed a proportional relationship of the added resistance to the square of wave amplitude and stated the superposition principle. The basis was then extended to the momentum conservation method, which is derived from the momentum balance through the control volume around ship hull (Maruo, 1960, 1963). The radiated energy method originally developed by Gerritsma and Beukelman (1972) was further implemented by Salvesen (1978). In parallel to these works, Faltinsen et al. (1980) proposed the asymptotic added resistance calculation formula for wall-side ship hull in short wave.

The aforementioned methods are relatively complicated, which more or less rely on the conventional potential flow and strip theory to obtain ship motion response. The motion is the first order problem of wave amplitudes, but a minor motion difference can lead to a significant deviation of the second order resistance in the numerical analysis. In the short wave region, the potential flow theory has even reached its limit due to the inevitable viscous effect. The calculations normally overestimate the added resistance peak in the long wave region and underestimate such resistances in short waves. In addition, the time requirement for using those methods is typical in minutes to estimate the resistance at a specific sea state (ITTC, 2018). However, energy efficient measures to guide a ship's operation often require immediate answers because estimation in tremendous sea states are often needed, such as in ship performance monitoring systems, ship voyage optimization systems, etc. Therefore, it is necessary to develop fast semi-empirical methods for calculating the wave added resistance with satisfactory accuracy, while the IMO has also called for the simplified formula and divided the development into three different states (IMO, 2013):

- level 1, the regular head wave;
- level 2, the regular incident waves with arbitrary angles;
- level 3, the irregular wave field scenario.

In 1975, Fujii and Takahashi (1975) proposed a well-recognized formula, namely the NMRI (National Maritime Research Institute of Japan) formula, for diffraction dominated wave added resistance based on the theoretical solutions from Ursell and Dean (1947). Simultaneously, a semi-empirical method was proposed by Jinkine and Ferdinande (1974) to calculate added resistance due to waves in the long wave region for fast cargo ships. MARIN continued to extend the method to short wave, and proposed the STAwave-1 as well as STAwave-2 formula, with additional measurement data and recommended by the International Towing Tank Conference (ITTC, 2012; Grin, 2012). Besides, ITTC (2018) merged Maruo's theorem by introducing Kochin function in the NMRI formula, though it is still inefficient because of the mandatory sectional offset integration. Recently, further simplification and combination of the above methods, Liu and Papanikolaou (2016a), Liu et al. (2016) proposed a fast approach based on large public available experiment results with a good estimation capability (denoted as NTUA-SDL Simpl. or NTUA method).

The NTUA method has improved the estimation accuracy of the added resistance in the regular head wave compared to the STAwave-2 method, but it still cannot give good prediction in comparison with the test resistances of the HSVA cruise, KVLCC2 tanker and DTC containership, particularly for the tail area of short waves with $\lambda/L_{pp} < 0.3$ as shown in Fig. 2, where R_{aw} is the added resistance due to various regular waves. Furthermore, as the increase of today's ship size, the short wave region with lower λ/L_{pp} value has become more crucial. Moreover, most of the aforementioned formulas have been proposed validated by model test results. There is a lack of public evidence to show their capabilities for predicting a ship's resistance in actual sea environments based on full-scale measurement data.

In this study, a new semi-empirical approach is proposed by combining the NMRI method (Fujii and Takahashi, 1975) for the added resistance in short waves and the method from Jinkine and Ferdinande (1974) for the resistance in long waves. Furthermore, some variables and tuning parameters are introduced in these two methods to better describe a ship's response behavior under different wave regions. The estimation by the proposed method for wave induced added resistance in the level 1 regular head wave has been compared with the published experimental tests from 11 ships. The accuracy of the estimation has been improved with better fitted resistance curve than the NTUA and ITTC recommended STAwave-2 (denoted as ITTC-STA2) methods. Moreover, based on the calculation of added resistance under regular waves for the level 1, a preliminary correction parameter in terms

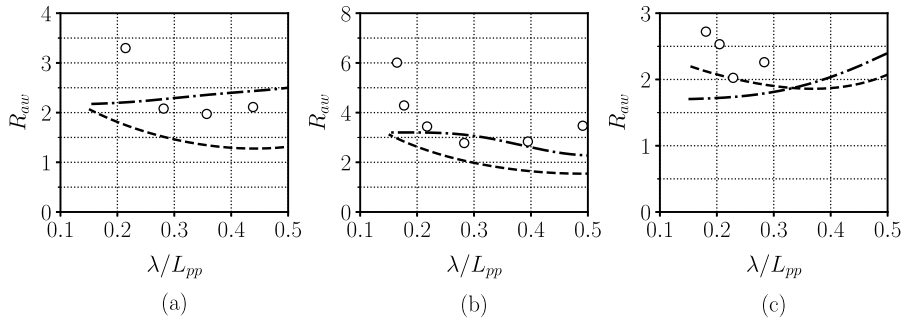

Fig. 2. Added resistance in the regular head wave, ○ experiment data, and calculated by ITTC-STA2, NTUA; estimated for (a) DTC container of $F_n = 0.139$, (b) HSVA cruise of $F_n = 0.232$, (c) KVLCC2 tanker of $F_n = 0.050$.

of significant wave height is proposed to add in the conventional integration method to estimate the added resistance under "actual" sea states (irregular waves in the level 3). This parameter is supposed to consider the severe coupled ship motions in harsher sea conditions. Finally, the capability of the proposed method for estimating wave induced added resistance and speed loss in actual head sea operations is validated, showing good agreement with full-scale measurements from two ships, i.e., one Pure Car Truck Carrier (PCTC) and a chemical tanker. Some measured ship operation related parameters, such as the position, heading, speed, draft and the engine power are adopted for the validation.

The left part of the paper is organized as follows to describe the proposed method. In Section 2, the detailed theoretical speed loss estimation model is proposed. Section 3 presents the development of the proposed semi-empirical method to estimate added resistance in regular head waves. The proposed method is validated using experimental test data in Section 4. Section 5 validates the proposed methods using full-scale measurement data. The results are discussed about the prediction capacity of the proposed method and the uncertainties in Section 6.

2. Theoretical estimation procedure for speed loss prediction

In order to predict a ship's speed loss when sailing in certain sea environments, it is essential to estimate the ship's actual sailing V_{real} speed under the specific sea conditions and "imaginary" speeds V_{calm} under calm water conditions for a given engine power. As Fig. 3 illustrates, the workflow to get such speeds at sea is an iterative process where the initial ship speed is one of the key parameters that determine the estimation, similar to the velocity prediction program (VPP) (de Jong et al., 2009).

In comparison with estimating a ship's sailing speeds at a specific sea state, it is relatively easy to get the calm water speed V_{calm}. The relationship between V_{calm} and engine power is often given by shipyards as a baseline to guide a ship's navigation and voyage planning. For a specific engine setting $P_{setting}$, the calm water speed V_{calm} can be interpolated from the given baseline.

In the iterative process for calculation of V_{real}, the V_{calm} is set as the initial value for the estimation of V_{real} for actually encountered sea states at the specific engine power. Then, a small adjustment $V_{adjustment}$ is added to the input V_{calm} to form a guess ship speed, which is used to estimate the ship's total resistance and consequently the required power $P_{prediction}$. When the absolute difference between the specific engine power $P_{setting}$ and the calculated engine power $P_{prediction}$ is less than 5% of $P_{setting}$, the iterative process stops. The final input ship speed is outputted as the V_{real} for that specific engine power under the given sea (wind and wave) condition. Finally, the speed loss can be simply evaluated by Eq. (1).

As shown in the red box of Fig. 3, an accurate module to describe a ship's resistance and propulsion system is essential for the entire estimation process. In the following, basic ship propulsion models used in this study is briefly presented, while special focus is put on the formulas for the added resistance due to head waves.

2.1. General concept of ship propulsion

A ship's resistance and propulsion systems contain two main modules, i.e., total resistance, and propulsion efficiencies. Let R_{TOTAL} denote the total resistance ships suffered when sailing in a seaway. The power required to push a ship to overtake her total resistance, with a forward speed through water V, is called the effective power P_e:

$$P_e = R_{TOTAL} \times V \tag{2}$$

The effective power P_e is transmitted from a ship's engine brake power P_b through her shaft system with a shaft transmission efficiency η_S and propeller in water with the propulsive efficiency η_D as follows (Carlton, 2012):

$$P_e = P_b \cdot \eta_S \cdot \eta_D \tag{3}$$

where η_S is normally with values around 0.98 to 0.99. In this study, η_S is assumed to be 1 for the following analysis. The total resistance is typically divided into the calm water resistance R_{CALM}, added resistance due to wave R_{AW} and wind R_{AA}:

$$R_{TOTAL} = R_{CALM} + R_{AA} + R_{AW} \tag{4}$$

Accurate calculation of these ship resistance is essential to get a reliable ship speed–power performance model when sailing in a seaway.

2.2. Calm water resistance and added resistance due to wind

An approximate calm water resistance calculation method was proposed by Holtrop and Mennen (1982), based on full-scale trails and model experiment. The method accounts for the ship main dimensions, ship type, appendage arrangement, immersed transom sterns, and the total resistance in still water is divided into six different components as:

$$R_{CALM} = R_F(1 + k_1) + R_{APP} + R_W + R_B + R_{TR} + R_A \tag{5}$$

where R_F is the frictional resistance here estimated by the ITTC-1957 frictional correlation curve (ITTC, 2002), and the form factor $1 + k_1$, the resistance of appendages R_{APP}, wave resistance of bare hull R_W, additional resistance from immersed transom R_{TR}, model-ship correlation resistance R_A are calculated by empirical formulas. The additional pressure resistance R_B due to a bulbous bow presence near the water surface needs to be investigated, while the wave resistance R_W should consider a reduction due to the action of the bulbous bow as empirical formulas.

The added resistance due to wind R_{AA} is dependent on the area of structure above the waterline as well as the relative wind speed (Lewis, 1988). In this study, it is estimated by the formula given by the International Organization Standardization (ISO, 2015):

$$R_{AA} = \frac{1}{2}\rho_A C_{AA}\left(\psi_{WR}\right) A_{XV} {V_{WR}}^2 \tag{6}$$

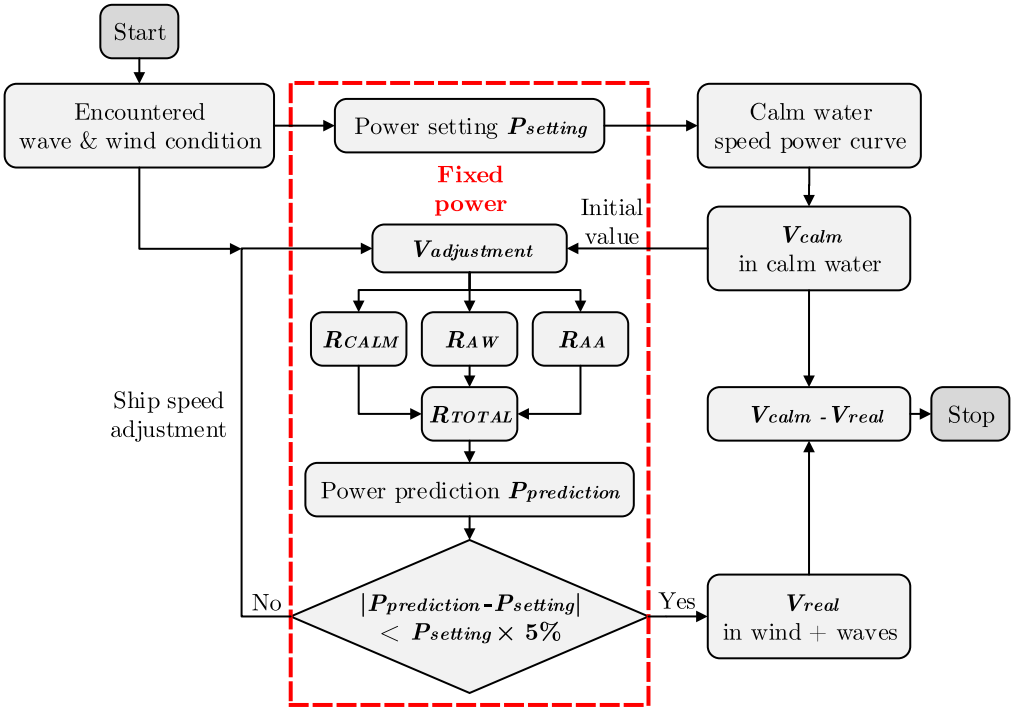

Fig. 3. Flowchart of the proposed theoretical weather factor prediction model.

where ρ_A is the air mass density, A_{XV} is the transverse projected area above waterline including superstructures, V_{WR} is the relative wind speed, ψ_{WR} is the relative wind direction, C_{AA} are the wind resistance coefficients for various heading angles obtained from wind tunnel model tests.

2.3. Added resistance due to waves under a practical sea state

The estimation of a ship's added resistance due to waves R_{AW} under actual sea states (irregular waves) often starts with getting the wave resistance under a series of regular waves with frequency w with wave amplitude $\zeta_a(\omega)$, i.e., $R_{aw}(\omega)$, which can be obtained by either experimental tests, semi-empirical models, or even numerical calculations. Note that the resistance R_{AW} should also be dependent on a ship's wave heading/attacking angles. This study only investigates the resistance in the head wave operations as in Liu and Papanikolaou (2016a), and the heading angle is therefore neglected for the simplicity of the following descriptions. An actual sea state is normally described by a wave spectrum such as the Pierson–Moskowitz wave spectrum (Pierson and Moskowitz, 1964) dependent on the significant wave height H_s, wave peak period T_p. Sometimes an extra peak enhancement factor γ is added to the spectrum to allow for flexible spectrum shapes such as the JONSWAP spectrum (Hasselmann et al., 1973). In this study, the JONSWAP spectrum is used for the added wave resistance estimations and expressed by:

$$S(\omega|H_s,T_p,\gamma)=\frac{320{H_s}^2}{{T_p}^4\omega^5}\exp\left(\frac{-1950}{{T_p}^4\omega^4}\right)\gamma^{\exp\left[\frac{-(\omega-\omega_p)^2}{2\sigma^2\omega_p{}^2}\right]} \tag{7}$$

while the spectral width parameters $\sigma = 0.07$ for $\omega \leqslant \omega_p$, $\sigma = 0.09$ when $\omega > \omega_p$. The newly developed semi-empirical head wave added resistance formula has been applied in this study, which is derived in the following section.

For a given sea state of wave spectrum $S(\omega|H_s,T_p,\gamma)$, the added resistance due to its irregular waves can be estimated by the linear integration of the resistances from its regular wave components of all wave frequencies as shown:

$$R_{AW}(H_s,T_p,\gamma)=2\int_0^\infty S(\omega|H_s,T_p,\gamma)\frac{R_{aw}(w)}{\zeta_a(\omega)^2}d\omega \tag{8}$$

It should be noted that since the main focus of this study is to investigate and propose various methods/formulas for getting the "accurate" added resistance due to waves and the corresponding ship speed loss. To mitigate the effect of possible errors from methods in getting R_{CALM} and R_{AA} for the case study ship of full-scale measurements, the results from the towing tank tests and wind tunnel measurements are used to get the corresponding calm water resistance and the wind resistance coefficients for this ship.

3. Improved semi-empirical models for $R_{aw}(\omega)$ in head waves

Added resistance due to waves is generally regarded as a non-viscous phenomenon. The added resistance in regular waves (again in head waves) of frequency ω can be separated into two components, i.e., added resistance due to wave reflection $R_{awr}(\omega)$, and added resistance due to ship motions $R_{awm}(\omega)$ (Strom-Tejsen et al., 1973):

$$R_{aw}(\omega)=R_{awr}(\omega)+R_{awm}(\omega) \tag{9}$$

where R_{awr} and R_{awm} are assumed to be uncoupled.

In this paper, it is recognized that the wave reflection induced resistance R_{awr} is mainly caused by short waves (large values of ω), while the wave motions induced resistance R_{awm} is mainly caused by long waves (small ω). Therefore, the development of models for R_{awr} focuses on short waves and for R_{awm} on long waves.

By inventorying all the recent development of semi-empirical formulas for these two added resistance components, it is concluded that the model of R_{awr} based on the NMRI formulas (Fujii and Takahashi, 1975) has a good capability to describe wave resistance in short waves. And for the added resistance due to wave induced motions R_{awm}, the model proposed by Jinkine and Ferdinande (1974) has a good description of wave resistance for long waves. Therefore, in this study, these two models are further developed to improve the accuracy of the semi-empirical models for the analysis of added resistance due to waves.

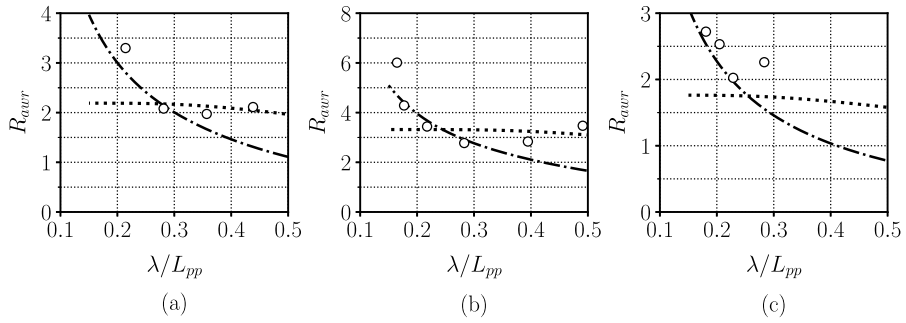

Fig. 4. Added resistance due to wave reflection in the regular head wave, ○ experiment data, and calculated by ▬·▬·▬ CTH, · · · · NMRI; estimated for (a) DTC container of $F_n = 0.139$, (b) HSVA cruise of $F_n = 0.232$, (c) KVLCC2 tanker of $F_n = 0.050$.

3.1. Improved models for added resistance due to wave reflection

The original NMRI semi-empirical formula to compute the added resistance due to wave was initially introduced four decades ago by Fujii and Takahashi (1975). Now it is adopted to compute added resistance due to wave reflections (for short waves) by:

$$R_{awr-NMRI} = \frac{1}{2}\rho g \zeta_a^2 B B_f \alpha_T \left(1 + \alpha_U\right) \tag{10}$$

where the fluid density ρ, gravitational acceleration g, ship width B, bluntness coefficient B_f, draft coefficient α_T and advance coefficient $(1+\alpha_U)$. The advance coefficient $(1+\alpha_U)$ was further developed (Takahashi, 1988; Kuroda et al., 2008; Tsujimoto et al., 2008) based on the supplementary experiment data as:

$$1 + \alpha_U = 1 + C_U F_n, \text{ where } C_U = \max(-310 B_f + 68, 10) \tag{11}$$

while C_U is correlated to the bluntness coefficient. The bluntness coefficient B_f is always estimated by integration method considering the shape of the water plane as well as wave direction. The value of B_f is highly correlated to the block coefficient C_B and can be simplified as an approximation expression (Liu and Papanikolaou, 2016a):

$$B_f = 2.25 \sin^2 E \tag{12}$$

The average entrance angle E is defined by ship width B and length of entrance L_E:

$$E = \arctan(B/2L_E) \tag{13}$$

Different from the original NMRI formula, the length of entrance L_E has been modified to be the length between the fore perpendicular and the point where it reaches 99% ship width at the waterline surface in Liu et al. (2016). In addition, instead of using Bessel function to estimate the draft coefficient α_T as in the NMRI model, it is modified to $\alpha_T = 1 - e^{-2kT}$ considering the fact that the exponential decay is observed to be more equivalent to the real physical wave energy dissipation (Liu et al., 2016; Valanto and Hong, 2015).

Although the original NMRI semi-empirical models have been continuously further developed to better estimate the added resistance due to wave reflections, it has a weak theoretical estimation capacity in the short wave region, especially when $\lambda < 0.3L_{pp}$. More specifically, it cannot catch up with the tail increase for the high frequency (short) wave reflections. For example, this weakness of the NMRI models is presented in Fig. 4 for the model tests from DTC container, KVLCC2 tanker and HSVA cruise model presented in, e.g., Liu et al. (2016), Valanto and Hong (2015), Liu and Papanikolaou (2016b), Guo and Steen (2011), Sadat-Hosseini et al. (2013), Moctar et al. (2015).

Therefore, in this paper, a wave length correction factor was tuned and added in the original NMRI semi-empirical model viz.:

$$R_{awr} = \frac{1}{2}\rho g \zeta_a^2 B B_f \alpha_T \left(1 + \alpha_U\right) \left(\frac{0.19}{C_B}\right)\left(\frac{\lambda}{L_{pp}}\right)^{F_n - 1.11} \tag{14}$$

where the wave length correction factor is settled by block coefficient C_B, Froude number F_n, and the ratio between wave length λ and ship length L_{pp}. Furthermore, k_eT is proposed to replace kT as the non-dimensional frequency in the draft coefficient:

$$\alpha_T = 1 - e^{-2k_eT} \tag{15}$$

where $k_e = k(1 + \Omega\cos\beta)^2$ and $\Omega = \frac{\omega V}{g}$, the circular frequency of incident regular waves ω, wave number of incident regular waves k.

The new modified formulas have presented more flexible prediction performance in the short wave region as shown in Fig. 4, where the proposed formula of Eq. (14) in this study is denoted as CTH. This flexible formula can help to match the reasonable resistance increase in the extremely short wave regions.

3.2. Improved models for added resistance due to ship motions

In parallel to the research development of added wave resistance by Fujii and Takahashi (1975) during the 1970s, a separate semi-empirical model was developed by Jinkine and Ferdinande (1974) based on the experiment data of a fine hull fast cargo ship. This model is found to be a reasonable approximation of added resistance for long waves, and often used as a basis for the succeeding development in e.g., ITTC and other research communities, to estimate added wave resistance due to ship motions. The original model is written as:

$$R_{awm-JF} = 4\rho g \zeta_a^2 B^2 / L_{pp} \overline{\omega}^{b_1} \exp\left[\frac{b_1}{d_1}\left(1 - \overline{\omega}^{d_1}\right)\right] a_1 a_2 \tag{16}$$

where a_1 is the amplitude factor, a_2 is the speed correction factor, b_1 and d_1 are the slope adjustment factors, and $\overline{\omega}$ is the frequency factor. The amplitude factor, originally proposed by Jinkine and Ferdinande (1974) has been continually modified. The most recent development was proposed by Liu and Papanikolaou (2016a), and further tuned in this study and expressed by:

$$a_1 = 60.3 {C_B}^{1.34} \left(\frac{1}{C_B}\right)^{1+F_n} \tag{17}$$

while block coefficient C_B and Froude number F_n were used as modification parameters. The speed correction factor a_2 in Eq. (16) has also been extended to the speed span of $0 \leqslant F_n \leqslant 0.3$, compared to the original high speed domain (ITTC, 2012; Grin, 2012; Liu and Papanikolaou, 2016a).

In this study, through the careful analysis of all collected experimental data, it is found that the speed correction factor a_2 is susceptible to the longitudinal radius of gyration k_{yy} and the block coefficient C_B in high speed region, and it has a little bit steeper slope compared to the NTUA formula when $F_n < 0.12$. Hence, the following formula is consequently proposed:

$$a_2 = \begin{cases} 0.0072 + 0.24F_n & \text{for } F_n < 0.12 \\ {F_n}^{-1.05C_B+2.3} \exp((-2 - \lceil \frac{k_{yy}}{0.25} \rceil - \lfloor \frac{k_{yy}}{0.25} \rfloor) F_n) & \text{for } F_n \geq 0.12 \end{cases} \tag{18}$$

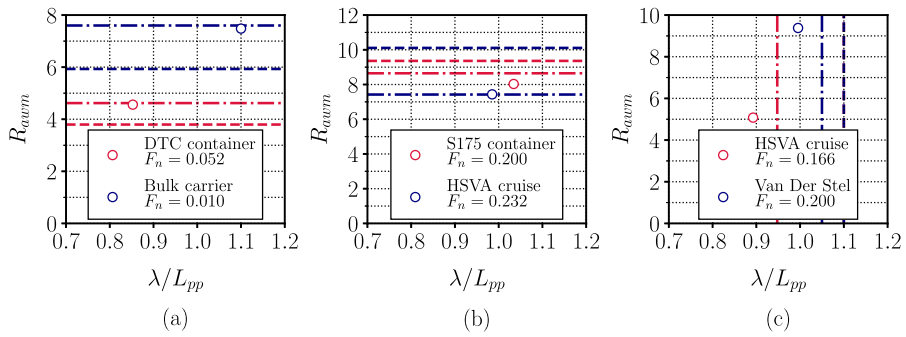

Fig. 5. Added resistance due to ship motions in the regular head wave, ○ experiment data, the horizontal line is the peak value, and the vertical line is the resonance position calculated by ▬·▬·▬ CTH, ▬ ▬ ▬ NTUA.

where the ceiling function $\lceil \frac{k_{yy}}{0.25} \rceil$ and floor function $\lfloor \frac{k_{yy}}{0.25} \rfloor$ can give discrete scales for F_n, concerning the correlation between k_{yy} and the typical value 0.25 (ITTC, 2017). The proposed Eq. (18) can consider the k_{yy} variation for different types of ships. The value of k_{yy} is fitted with the peak value of those experiment measurements. The improvement for estimating added resistance due to ship motions R_{awm} is presented as 6 cases in Fig. 5. For example, Fig. 5(a) shows the comparison between the NTUA method and the proposed method with two model tests for $F_n < 0.12$, while Fig. 5(b) presents two comparison cases for $F_n \geq 0.12$.

The frequency factor $\overline{\omega}$ is determined by the frequency of heave and pitch motions, which resonance response of these motions is regarded as the leading cause of radiation induced added resistance reaching the peak value in head sea. Liu and Papanikolaou (2016a) separated the expression to lower and normal speed, whereas it is still not able to match the experimental data well for some cases when k_{yy} do not equal to 0.25, especially for HSVA cruise (Valanto and Hong, 2015). It is also observed that the resonance frequency moves horizontally from $\lambda/L_{pp} < 1$ to $\lambda/L_{pp} > 1$ as the Froude number F_n increase. The trend is influenced by the longitudinal radius of gyration variation as well. Consequently, the expression is further parameter tuned in this study, and the modified formula is given by:

$$\overline{\omega} = \begin{cases} \dfrac{\sqrt{L_{pp}/g}\, c_1 \sqrt{\frac{k_{yy}}{L_{pp}}}\, 0.05^{0.143}}{1.09 + \lceil \frac{k_{yy}}{0.25} \rceil 0.08}\omega & \text{for } F_n < 0.05 \\ \dfrac{\sqrt{L_{pp}/g}\, c_1 \sqrt{\frac{k_{yy}}{L_{pp}}}\, F_n^{0.143}}{1.09 + \lceil \frac{k_{yy}}{0.25} \rceil 0.08}\omega & \text{for } F_n \geq 0.05 \end{cases} \tag{19}$$

where the root $c_1 = 0.4567\frac{C_B}{k_{yy}} + 1.689$, and the improved expression results are closer to the resonance position (assumed as the highest resistance position) in experiment measurements, as shown in Fig. 5(c). Furthermore, in this study, the slope adjustment is also calibrated with respect to the longitudinal radius of gyration k_{yy} and the block coefficient C_B:

$$b_1 = \begin{cases} (19.77\frac{C_B}{k_{yy}} - 36.39)/\lceil \frac{k_{yy}}{0.25} \rceil & \text{for } \overline{\omega} < 1, C_B < 0.75 \\ 11/\lceil \frac{k_{yy}}{0.25} \rceil & \text{for } \overline{\omega} < 1, C_B \geqslant 0.75 \\ -12.5/\lceil \frac{k_{yy}}{0.25} \rceil & \text{for } \overline{\omega} \geqslant 1, C_B < 0.75 \\ -5.5/\lceil \frac{k_{yy}}{0.25} \rceil & \text{for } \overline{\omega} \geqslant 1, C_B \geqslant 0.75 \end{cases} \tag{20}$$

$$d_1 = \begin{cases} 14 & \text{for } \overline{\omega} < 1, C_B < 0.75 \\ 566\left(\frac{L_{pp}}{B}\right)^{-2.66} \cdot 2 & \text{for } \overline{\omega} < 1, C_B \geqslant 0.75 \\ -566\left(\frac{L_{pp}}{B}\right)^{-2.66} \cdot 6 & \text{elsewhere} \end{cases} \tag{21}$$

while $C_B = 0.75$ is adopted as the boundary to define the piece-wise. The final calculated non-dimensional curves demonstrate much better slope, peak matching to the model tests.

3.3. The proposed semi-empirical model for R_{aw}

In this study, a wave length correction is proposed to be added in the NMRI semi-empirical model (Fujii and Takahashi, 1975), whose draft coefficient is also further modified to consider actual wave energy dissipation when sailing in waves. This model is used to estimate added resistance in short waves, i.e., due to wave reflections R_{awr} in Eq. (9). Furthermore, the semi-empirical model by Jinkine and Ferdinande (1974) is further developed by improving the speed correction factor a_2, frequency factor $\overline{\omega}$, slope adjustment b_1 and d_1. The latter developed model is used to estimate added resistance in long waves, i.e., due to wave motions R_{awm} in Eq. (9). The summation of the two models leads to the total added resistance due to waves as in Eq. (9). To summary, the evolution of present development of the added resistance R_{aw} for head waves, the entire semi-empirical model proposed in this study (denoted as the CTH model) is listed in Box I.

4. Validation of the proposed model using model tests in regular head waves

The proposed semi-empirical model in Section 3 is compared with the aforementioned ITTC-STA2, NTUA method for the estimation of added resistance in head waves. A number of available ship model test measurements were collected to validate the proposal model, i.e., S175 container (Fujii and Takahashi, 1975; Takahashi, 1988), KVLCC2 tanker (Guo and Steen, 2011; Sadat-Hosseini et al., 2013), DTC container (Liu and Papanikolaou, 2016b; Moctar et al., 2012), HSVA cruise (Valanto and Hong, 2015), S.A. Van Der Stel (Alexandersson, 2009), a bulk carrier (Kadomatsu, 1988), and Series 60 models with five various block coefficient C_B (Strom-Tejsen et al., 1973). All the required parameters of these studied ships required in the semi-empirical models are listed in Table 1.

For the validation of the proposal semi-empirical model and comparison with other methods, in addition to illustrated figures to plot the estimated resistance R_{aw} against the model test results, the mean squared error (MSE by Hastie et al. (2009)) is used as an estimator to quantitatively compare the accuracy of those models. For each ship model test at a given speed F_n under a series of regular waves with frequency ω_i, $i = 1, 2, \ldots, n$, the MSE can be calculated by:

$$\text{MSE} = \frac{1}{n}\sum_{i=1}^{n}\left(R_{aw}(\omega_i) - \widehat{R_{aw}(\omega_i)}\right)^2 \tag{22}$$

where $R_{aw}(\omega_i)$ represents the measured resistance, and $\widehat{R_{aw}(\omega_i)}$ represents the estimated resistance, such as by Eq. (9), or the NTUA, ITTC-STA2 methods.

Some typical model test cases selected from six different ships are presented in Fig. 6, which presents the added resistance due to waves R_{aw} estimated by the proposed method, the ITTC-STA2 method and the NTUA method, in comparison with the model test results. (The comparison of those methods for all the available test ships listed in

$$R_{aw} = R_{awr} + R_{awm}$$

$$R_{awr} = \frac{1}{2}\rho g \zeta_a^2 B B_f \alpha_T \left(1+\alpha_U\right)\left(\frac{0.19}{C_B}\right)\left(\frac{\lambda}{L_{pp}}\right)^{F_n-1.11}$$

$$B_f = 2.25\sin^2 E, \text{ where } E = \arctan(B/2L_E)$$

$$1+\alpha_U = 1 + C_U F_n, \text{ where } C_U = \max(-310B_f + 68, 10)$$

$$\alpha_T = 1 - e^{-2k_e T}, \text{ where } k_e = k(1+\Omega\cos\beta)^2 \text{ and } \Omega = \frac{\omega V}{g}$$

$$R_{awm} = 4\rho g \zeta_a^2 B^2 / L_{pp} \overline{\omega}^{b_1} \exp\left[\frac{b_1}{d_1}\left(1-\overline{\omega}^{d_1}\right)\right] a_1 a_2$$

$$a_1 = 60.3 {C_B}^{1.34}\left(\frac{1}{C_B}\right)^{1+F_n}$$

$$a_2 = \begin{cases} 0.0072 + 0.24F_n & \text{for } F_n < 0.12 \\ F_n^{-1.05C_B+2.3}\exp((-2-\lceil\frac{k_{yy}}{0.25}\rceil - \lfloor\frac{k_{yy}}{0.25}\rfloor)F_n) & \text{for } F_n \geq 0.12 \end{cases}$$

$$\overline{\omega} = \begin{cases} \dfrac{\sqrt{L_{pp}/g}\, c_1 \sqrt{\frac{k_{yy}}{L_{pp}}}\, 0.05^{0.143}}{1.09 + \lceil\frac{k_{yy}}{0.25}\rceil 0.08}\omega & \text{for } F_n < 0.05 \\ \dfrac{\sqrt{L_{pp}/g}\, c_1 \sqrt{\frac{k_{yy}}{L_{pp}}}\, F_n^{0.143}}{1.09 + \lceil\frac{k_{yy}}{0.25}\rceil 0.08}\omega & \text{for } F_n \geq 0.05 \end{cases} \quad \text{where } c_1 = 0.4567\frac{C_B}{k_{yy}} + 1.689$$

$$b_1 = \begin{cases} (19.77\frac{C_B}{k_{yy}} - 36.39)/\lceil\frac{k_{yy}}{0.25}\rceil & \text{for } \overline{\omega} < 1, C_B < 0.75 \\ 11/\lceil\frac{k_{yy}}{0.25}\rceil & \text{for } \overline{\omega} < 1, C_B \geqslant 0.75 \\ -12.5/\lceil\frac{k_{yy}}{0.25}\rceil & \text{for } \overline{\omega} \geqslant 1, C_B < 0.75 \\ -5.5/\lceil\frac{k_{yy}}{0.25}\rceil & \text{for } \overline{\omega} \geqslant 1, C_B \geqslant 0.75 \end{cases}$$

$$d_1 = \begin{cases} 14 & \text{for } \overline{\omega} < 1, C_B < 0.75 \\ 566\left(\frac{L_{pp}}{B}\right)^{-2.66}\cdot 2 & \text{for } \overline{\omega} < 1, C_B \geqslant 0.75 \\ -566\left(\frac{L_{pp}}{B}\right)^{-2.66}\cdot 6 & \text{elsewhere} \end{cases}$$

Box I.

Table 1
Main particulars of the studied ships in experiments from available publications.

Ship type	L_{pp} [m]	B [m]	T [m]	C_B [-]	L_E [m]	k_{yy} [-]
S175 container	175	25.4	9.5	0.572	59.05	0.24
KVLCC2 tanker	320	58	20.8	0.8098	60	0.25
DTC container	355	51	14.5	0.661	112	0.27
HSVA cruise	220.27	32.2	7.2	0.654	72.42	0.263
S.A. Van Der Stel	152.5	22.8	9.14	0.563	61	0.22
Bulk carrier	285	50	18.5	0.829	51	0.25
Series 60 model 4210	121.96	16.254	6.492	0.6	52	0.25
Series 60 model 4211	121.96	16.816	6.73	0.65	46.522	0.25
Series 60 model 4212	121.96	17.42	6.97	0.7	38.606	0.25
Series 60 model 4213	121.96	18.062	7.22	0.75	30.48	0.25
Series 60 model 4214	121.96	18.757	7.495	0.8	22.8	0.25

Table 1 are presented in the Appendix from Figs. A.13 to A.23.) As Fig. 6(c) shows, the proposed formula has significantly improved added resistance estimation for the HSVA cruise, either in the short wave field tail increase or the long wave field peak value seizing. Similarly, that has resulted in better performance in the resonance region and peak catching, for bulk carrier in Fig. 6(a) and S175 container in Fig. 6(e). The NTUA approach can surely catch the peak and the resonance region, whereas the prediction capacity in the short wave field cannot perform as well as the proposed formula. Obviously, the ITTC-STA2 method has underestimated for almost all cases.

Furthermore, the MSEs of the added resistance due to waves R_{aw} for the proposed (CTH) model, the ITTC-STA2 model, and the NTUA model are computed for all the experimental model tests. In order to have an easy comparison, all the computed MSEs are normalized in terms of the values from the proposed CTH formulas, and the corresponding results are listed in Table 2. It should be noted that large values of MSE mean bad estimation of that method in comparison with the proposed CTH formulas. As the table expresses, the proposed formulas in Section 3.3 have the best prediction performance for almost all the studied instances, expect 3 cases the best is the NTUA model and 1 case the best is the ITTC-STA2 model. In general, the proposed semi-empirical formulas have shown superior estimation ability than the other considered approaches for the level 1 wave resistance estimation under regular head sea conditions. Therefore, it was adopted in the

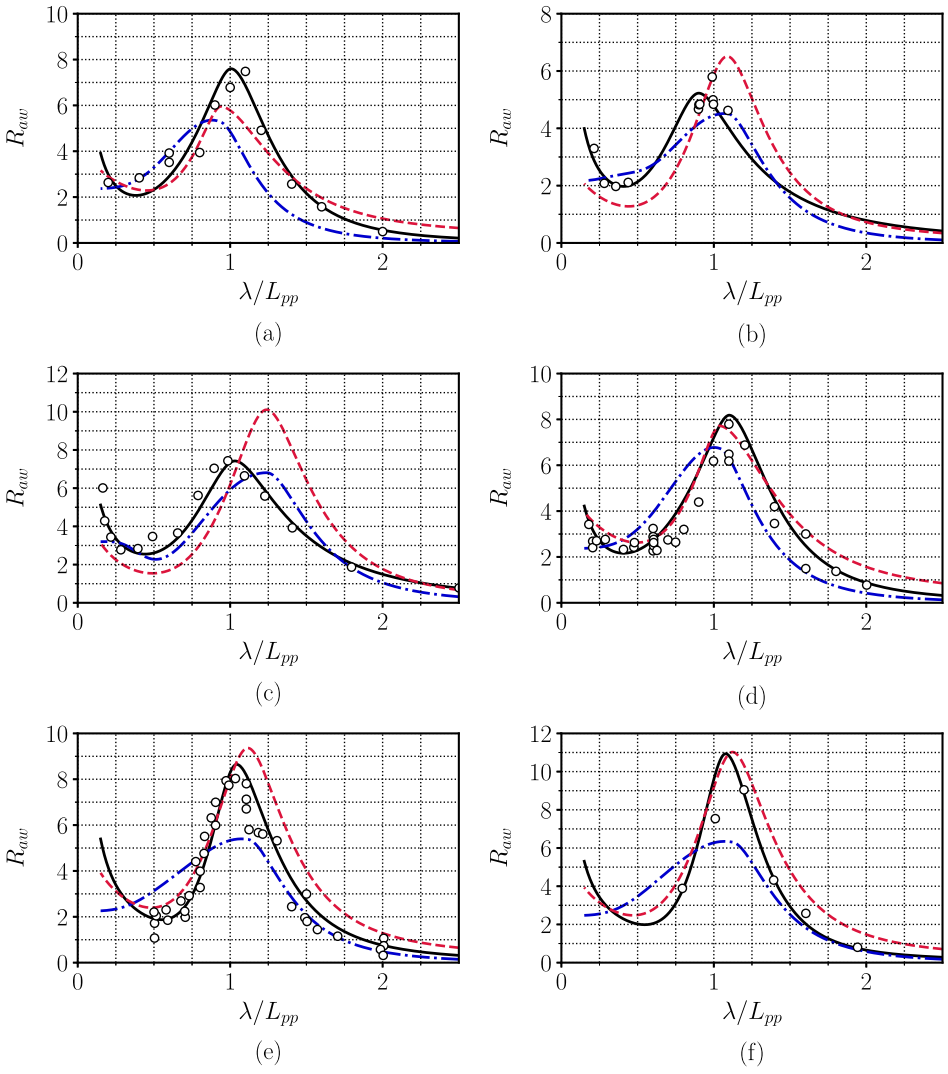

Fig. 6. Added resistance in the regular head wave, ○ experiment data, ——— CTH, -·-·- ITTC-STA2, - - - NTUA; estimated for (a) Bulk carrier of $F_n = 0.010$, (b) DTC container of $F_n = 0.139$, (c) HSVA cruise of $F_n = 0.232$, (d) KVLCC2 tanker of $F_n = 0.142$, (e) S175 container $F_n = 0.200$, (f) S.A. Van Der Stel of $F_n = 0.250$.

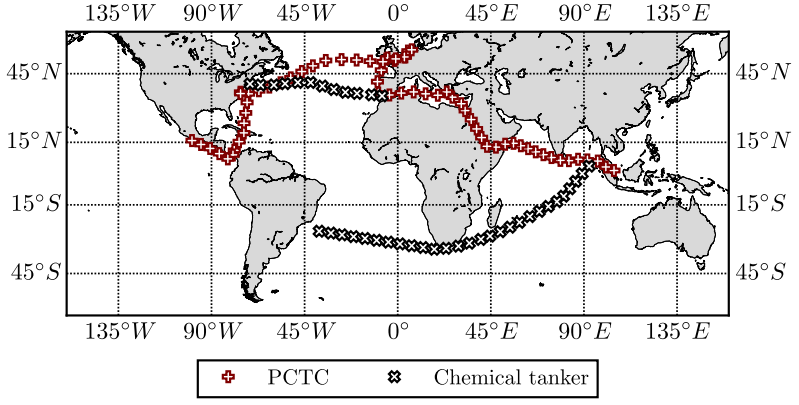

Fig. 7. Typical routes of the studied PCTC and chemical tanker during the measurement campaign.

Table 2
MSE analysis of entire experiment measurement validation cases in the regular head wave, all the outcomes are normalized by the proposed formula results.

Ship type	Froude number	CTH	NTUA	ITTC-STA2	Best fit
S175 container	0.150	1	2.34	4.84	CTH
	0.200	1	3.90	3.26	CTH
	0.250	1	1.82	2.86	CTH
	0.275	1	1.23	12.99	CTH
KVLCC2 tanker	0.050	1	3.28	9.40	CTH
	0.090	1	1.19	3.91	CTH
	0.142	1	1.02	2.77	CTH
	0.180	1	1.10	3.01	CTH
DTC container	0.052	1	1.69	5.63	CTH
	0.139	1	4.15	2.20	CTH
HSVA cruise	0.166	1	6.70	1.11	CTH
	0.232	1	17.11	5.29	CTH
S.A. Van Der Stel	0.150	1	0.27	1.52	NTUA
	0.200	1	0.38	4.00	NTUA
	0.250	1	2.15	2.65	CTH
	0.300	1	1.66	3.40	CTH
Bulk carrier	0.000	1	5.61	2.62	CTH
	0.005	1	0.77	0.74	ITTC-STA2
	0.010	1	2.15	5.75	CTH
	0.150	1	1.19	6.33	CTH
Series 60 model 4210	0.266	1	5.81	6.67	CTH
	0.283	1	1.54	1.33	CTH
Series 60 model 4211	0.237	1	2.13	5.79	CTH
	0.254	1	4.67	4.73	CTH
Series 60 model 4212	0.207	1	3.50	10.32	CTH
	0.222	1	3.08	3.61	CTH
Series 60 model 4213	0.177	1	1.37	3.43	CTH
	0.195	1	1.03	2.52	CTH
Series 60 model 4214	0.147	1	0.96	1.83	NTUA
	0.165	1	1.03	1.48	CTH

proposed speed loss prediction model to estimate added resistance due to waves. The capability of the speed loss prediction model will be investigated by full-scale measurements in the following analysis.

5. Model validation by full-scale measurements at actual head sea conditions

The full-scale measurements in this paper were recorded from one PCTC and one chemical tanker. They were instrumented with several sensors and equipment to collect a large amount of ship energy performance related data, up to a gigabyte per day. The main particulars of these two ships are shown in Table 3 and applied as inputs for the following ship resistance calculation.

For this study, the measurement data types from the two ships are quite similar. It includes the shaft power and torque along with the RPM from engine rooms, the ship draft from the stern and stem, longitude, latitude, speed over ground, speed through water, and ship headings, etc. along with the sailing voyages. The measurements were recorded with a frequency of 1 Hz, i.e., data collection every second. While the raw measurements are statistically evaluated every 15 min, and erroneous data is filtered. For example, several typical routes during the sailing recorded by the full-scale measurement campaign are illustrated in Fig. 7.

In addition to the two ships' main particulars and performance measurement data, their baselines obtained from model tests and sea trials, such as speed–power relationship in calm water conditions, wind resistance coefficients, etc., are provided by shipowners for this study, see Fig. 8. While the wind resistance coefficients C_{AA} measured through wind tunnel tests were adopted for the case study ships. The propulsive

Table 3
Main characteristics of the studied PCTC and chemical tanker for full-scale measurements.

Parameter	Symbol	Unit	PCTC	Chemical tanker
Length between perpendicular	L_{pp}	m	190	174.8
Breadth molded	B	m	32.26	32.2
Designed draft	T	m	9.5	10.98
Block coefficient	C_B	–	0.6	0.8005
longitudinal radius of gyration	k_{yy}	–	0.26	0.25
Length of entrance	L_E	m	62	40
Transverse projected area	A_{XV}	m^2	985	400
Deadweight	DWT	tonnes	28126	46067
Maximum continuous rating	P_c	kW	14700	8200

efficiency η_D is extracted from the ship model self-propulsion tests at the designed draft for various ship speeds, since only full loading condition is considered in this validation study. When full-scale measurements are used in this study, the η_D is interpolated from the self-propulsion tests for any measured ship speed. It should be noted that the propulsion efficiency η_D for a ship's actual sailing in waves should be different from that obtained from the experiment tests even for the same ship speed. In this study, the difference is included in the added resistance in waves.

5.1. Metocean data

For the prediction of a ship's energy performance in a seaway, it is the most essential to get accurate sea environments encountered along the ship's sailing routes. For these two case study ships, the

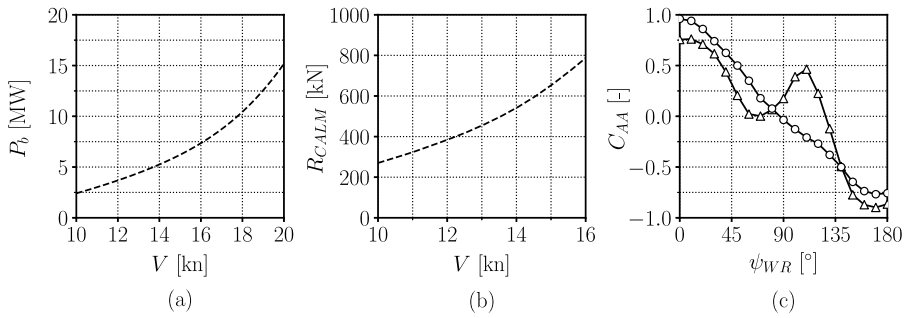

Fig. 8. Model tests results of (a) PCTC speed–power curve, (b) chemical tanker speed–calm water resistance curve, (c) wind resistance coefficient measurements for △ PCTC, while the value of ○ chemical tanker is adopted as ISO suggestion.

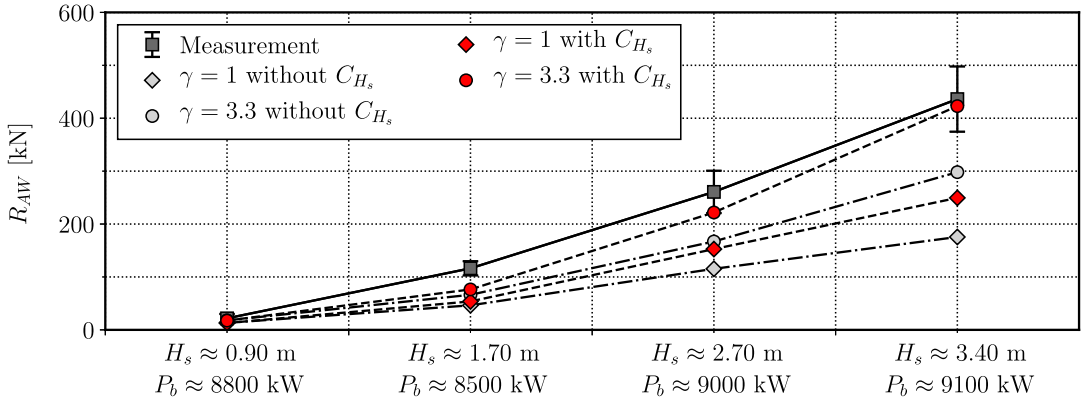

Fig. 9. The added resistance due to irregular head waves R_{AW} from measurements and estimated by the proposed model with Jonswap ($\gamma = 3.3$) and Pierson–Moskowitz ($\gamma = 1$) wave spectrum, with/without wave height correction factor $C_{H_s} = \sqrt[3.5]{H_s}$, for the PCTC under engine power setting close to 8800 kW.

encountered metocean environments, i.e., the mean wave direction D_{wave}, mean wave period T_z, significant wave height H_s, wind speed U_{wind} and V_{wind}, are extracted from the ECMWF reanalysis dataset ERA5 hourly with 0.25×0.25 degree spatial resolution (Copernicus, 2019). The information of current velocity $U_{current}$ and $V_{current}$ are obtained from the Copernicus Marine server, with the same geographical resolution, and the temporal resolution is 24 h (CMEMS, 2019). The extracted metocean environments from the hindcast datasets are assumed to be the actually encountered conditions. The two ships' loaded condition was pulled out from the huge amount of real measurements based on the draft analysis, and the relative wave angle along with wind angle were estimated. In order to decrease the uncertainty and enrich the studied dataset, the relative wave angle between 0° to 10° is considered as the head sea.

5.2. The wave height correction factor for wave resistance in head sea

Based on the analysis of added resistance in waves from the full-scale measurements of those two ships, it is found that there is a steeper rise in the added resistance as the significant wave height H_s increase, compared to the linear superposition calculation by the Eq. (8). It can be caused by the coupled ship motions in severe sea wave condition and rudder induced resistance controlled by the autopilot. Besides, the propulsion efficiency may also be reduced due to the big motions such as the propeller out of water. Consequently, a wave height correction factor $C_{H_s} = \sqrt[3.5]{H_s}$ was preliminary proposed and recommended in the added resistance estimation in the real irregular sea conditions viz:

$$R_{AW}(H_s, T_p, \gamma) = 2\int_0^\infty S(\omega|H_s, T_p, \gamma)\frac{R_{aw}(w)}{\zeta_a(\omega)^2}d_\omega \sqrt[3.5]{H_s} \tag{23}$$

In the following comparison analysis, for a chosen engine power, with the full-scale measurements of sailing speed and wave environments $[H_s, T_z]$ encountered by a case study ship, the added resistance due to waves R_{AW} can be estimated by the inverse procedure in Fig. 3. First, the propulsive efficiency η_D corresponding to the ship speed V is interpolated from the ship's self-propulsion tests. Then, the total resistance R_{TOTAL} is estimated from the engine power P_b, ship speed V and η_D by Eqs. (2) & (3). While R_{CALM} is interpolated from the ship's speed–power curve obtained from model tests. The added resistance due to wind R_{AA} is evaluated by the Eq. (6). The actual added resistance due to wave is calculated as $R_{AW} = R_{TOTAL} - R_{CALM} - R_{AA}$. Then an average value and the standard deviation of R_{AW} for the picked engine power, speed and wave condition are computed as the reference to be compared with the proposed method. The added resistance due to regular head waves R_{aw} under the same speed are calculated by the proposed method in Section 3.3. Finally, the added resistances under actually irregular sea state R_{AW} are computed by both the conventional method without wave height correction as Eq. (8) and the proposed method with wave height correction as Eq. (23), where the peak enhancement factor in the JONSWAP wave spectrum is chosen to be $\gamma = 3.3$ and $\gamma = 1$ (Pierson–Moskowitz spectrum) to investigate the sensitivity of R_{AW} to the shape of a wave spectrum. This calculation process is performed several times for various power, speed and wave conditions.

As shown in Fig. 9, the measurements with engine power around 8800 kW are used for the resistance verification for the studied PCTC. It has been sailing in calm sea conditions with a maximum significant wave height of less than 3.5 m. Four wave conditions with significant wave height, approximately 0.9 m, 1.7 m, 2.7 m, and 3.4 m are evaluated. Both the mean and standard deviation of R_{AW} from the measurements are presented in Fig. 9. Again, there is a sharp nonlinear increase of R_{AW} against the encountered significant wave height. The proposed semi-empirical models using wave spectrum with $\gamma = 3.3$ and wave height correction factor C_{H_s} gives very good results of R_{AW} in comparison with the measurement, although it has a little bit underestimation for $H_s \approx 1.7$ m.

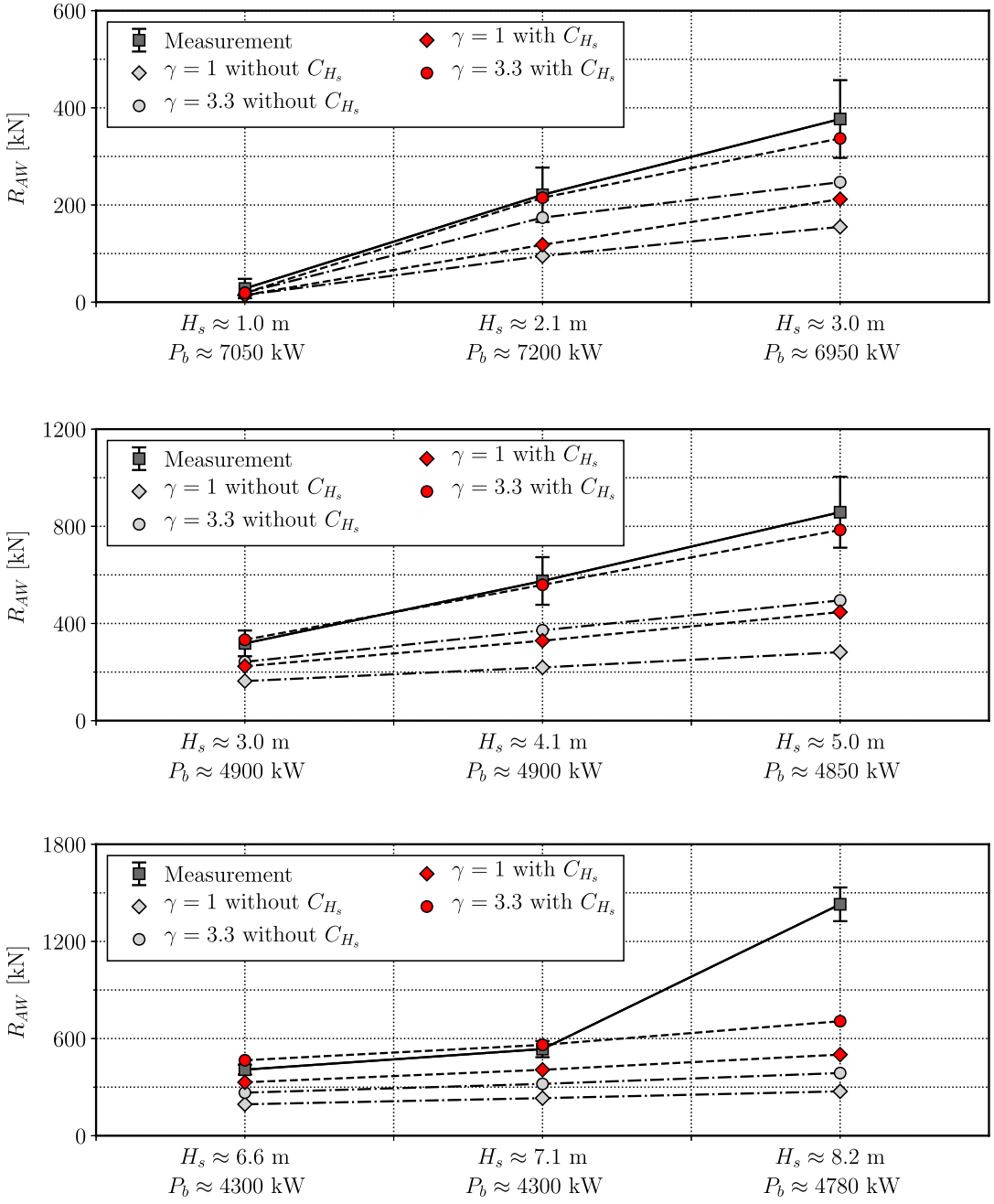

Fig. 10. The added resistance due to irregular head waves R_{AW} from measurements and estimated by the proposed model with Jonswap ($\gamma = 3.3$) and Pierson–Moskowitz ($\gamma = 1$) wave spectrum, with/without wave height correction factor $C_{H_s} = \sqrt[5]{H_s}$, for the chemical tanker under engine power setting Eco 2 (upper plot), Eco 5 (middle plot), and Eco 6 (bottom plot).

For the case study chemical tanker, a long time of full-scale measurement data is available in this study. Harsh encountered sea environments with H_s more than 8 m can be found from the measurement data. The chemical tanker is operated using a power-based navigation strategy, i.e., different power settings are used according to encountered sea conditions. The power setting onboard the ship is configured into various so-called Eco setting levels, such as Eco 2 setting (6660 kW to 7270 kW) for relative calm wave, Eco 5 setting (4830 kW to 5440 kW) for severer sea, and Eco 6 setting (4220 kW to 4830 kW) for harsh sea conditions. Similar calculations for the PCTC are performed for the chemical tanker at the above three engine Eco setting levels. The corresponding results are presented in Fig. 10.

It is again clearly indicated that the $\gamma = 3.3$ combined with the wave height correction factor has achieved the best prediction performance for almost all the studied cases, from H_s less than 1 m to H_s larger than 7 m. It was also observed that, except for the significant wave height and ship speed, the peak period has a vital influence on the added resistance in waves. For the cases $H_s \approx 6.6$ m and $H_s \approx 7.1$ m with Eco 6 setting, the wave period, is almost two times than the cases $H_s \approx 4.1$ m and $H_s \approx 5.0$ with Eco 5 setting, leading smaller resistance though they have larger wave height.

It should be noted that for the extraordinary case of $H_s \approx 8.2$ m in Fig. 10 (bottom plot), the added wave resistance R_{AW} estimated by the proposed method differs significantly from the measured values. The big difference might be caused by that the propulsion efficiency has been dramatically reduced due to the propeller out of the water surface under such large waves. Furthermore, another reason might be that the proposed wave height correction factor needed to be further increased to account for the extensive motions when sailing in so severe wave environments. In general, the proposed semi-empirical models as

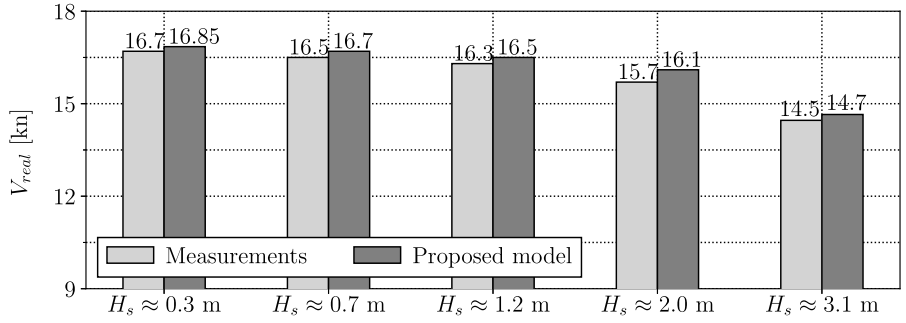

Fig. 11. The ship real speed comparison of the case study PCTC with various sea conditions; estimated for engine power setting around 8800 kW.

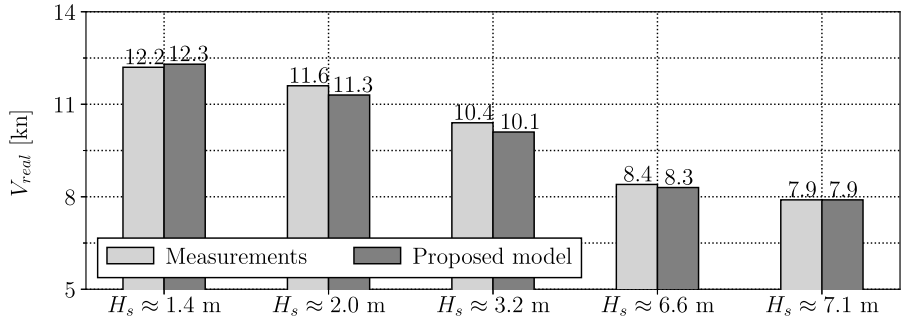

Fig. 12. The ship real speed comparison of the case study chemical tanker with various sea conditions; estimated for engine power setting around 4300 kW.

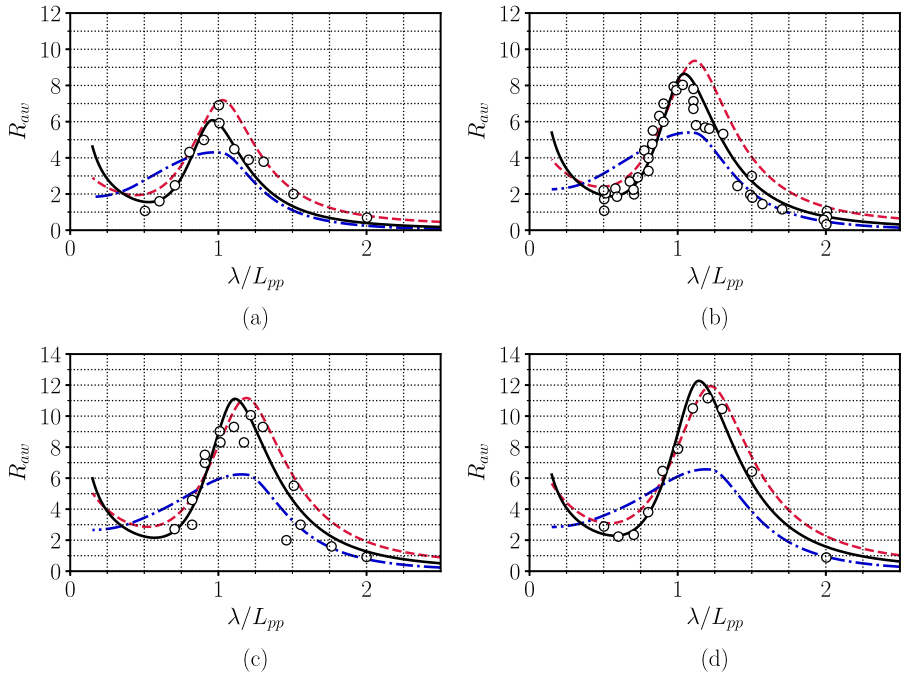

Fig. A.13. Added resistance of S175 container in the regular head wave, ○ experiment data, ——— CTH, -·-·- ITTC-STA2, - - - NTUA; estimated for (a) $F_n = 0.150$, (b) $F_n = 0.200$, (c) $F_n = 0.250$, (d) $F_n = 0.275$.

Eq. (23) with R_{aw} estimated by Eq. (9) gives quite good estimations of added wave resistance R_{AW} in comparison with measurement when a proper wave spectrum is used.

5.3. Validation of the proposed method for speed loss prediction by full-scale measurements

In order to check the accuracy of the proposed method for the prediction of a ship's speed loss when sailing in actual irregular head wave conditions, a fixed power for the case study ships should be first defined. Then, all the sailing waypoints encountering head waves are selected from the measurement data. In this study, the engine power of around 8800 kW (60% MCR) for the PCTC, and 4300 kW (52% MCR) for the chemical tanker, for the following speed loss analysis. The next is to divide all the selected waypoints into various groups based on their encountered wave environments. For example, for the PCTC ship, five groups of sea states are defined with significant wave heights H_s approximately to 0.3 m, 0.7 m, 1.2 m, 2.0 m, and 3.1 m. For the chemical tanker with long period of measurement data, five groups of

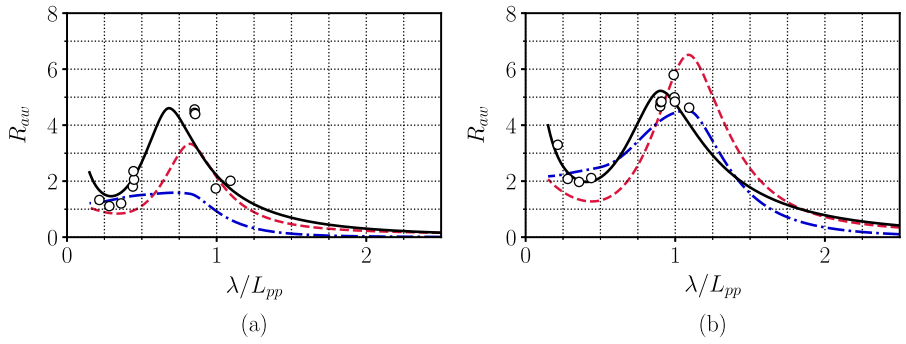

Fig. A.14. Added resistance of DTC container in the regular head wave, ○ experiment data, ——— CTH, -·-·- ITTC-STA2, - - - NTUA; estimated for (a) $F_n = 0.052$, (b) $F_n = 0.139$.

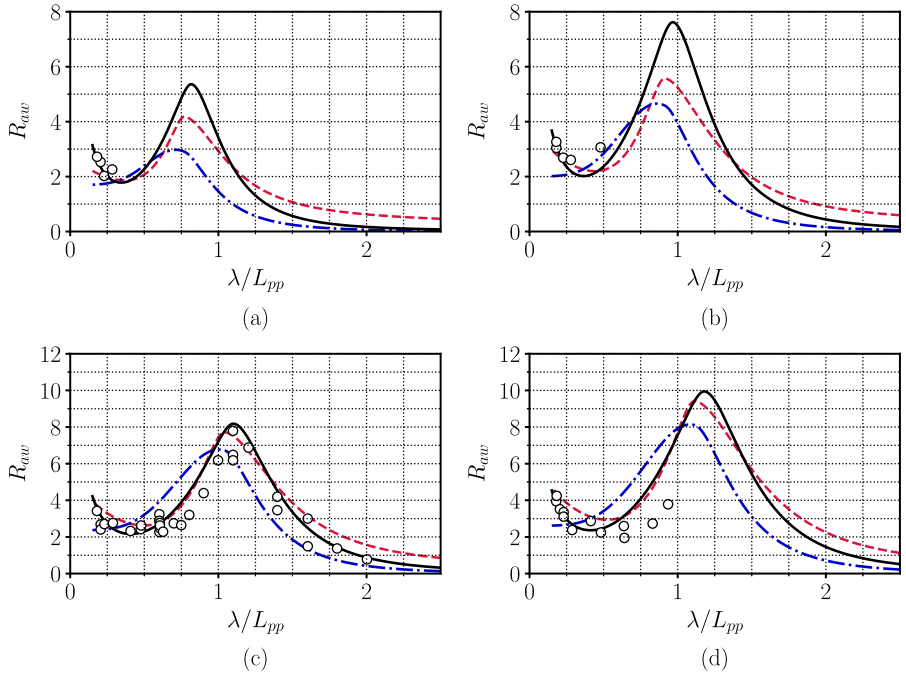

Fig. A.15. Added resistance of KVLCC2 tanker in the regular head wave, ○ experiment data, ——— CTH, -·-·- ITTC-STA2, - - - NTUA; estimated for (a) $F_n = 0.050$, (b) $F_n = 0.090$, (c) $F_n = 0.142$, (d) $F_n = 0.180$.

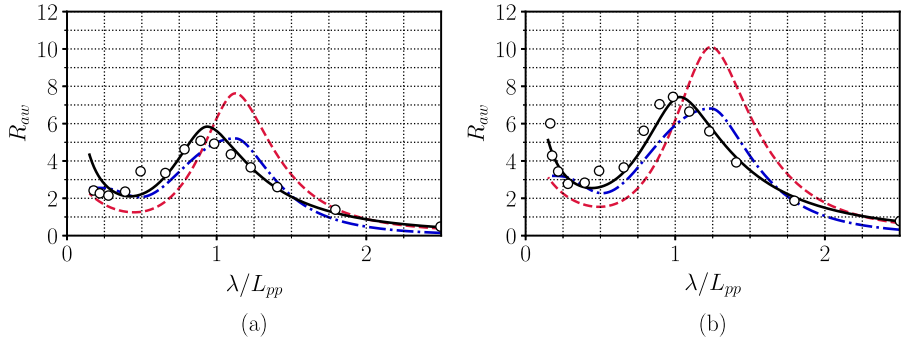

Fig. A.16. Added resistance of HSVA cruise in the regular head wave, ○ experiment data, ——— CTH, -·-·- ITTC-STA2, - - - NTUA; estimated for (a) $F_n = 0.166$, (b) $F_n = 0.232$.

more scattered sea states are defined with significant wave heights H_s approximately to 1.4 m, 2.0 m, 3.2 m, 6.6 m, and 7.1 m while the values of H_s within the range of ±0.05 m are regarded as the same sea states.

For the PCTC and the chemical tanker at the defined engine power settings, their speeds under calm water conditions V_{CALM} are computed to be 16.9 kn and 12.8 kn, respectively. Then, for each individual sea state, the real sailing speeds V_{real} are estimated using the procedures presented in Fig. 3, where the added resistance due to waves are estimated by the proposed method. Furthermore, the actual sailing speeds V_{real} under all these sea states are calculated as the mean values of the measured speeds for all those waypoints with the same sea state. The comparison of V_{real} between the measured mean values and the

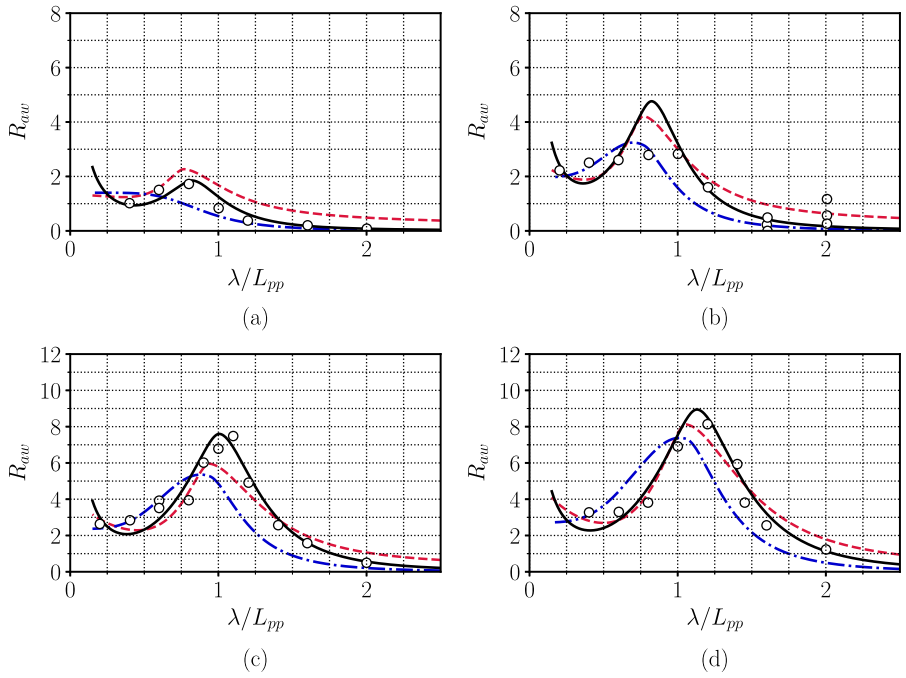

Fig. A.17. Added resistance of the studied bulk carrier in the regular head wave, ○ experiment data, ——— CTH, -·-·- ITTC-STA2, - - - NTUA; estimated for (a) $F_n = 0$, (b) $F_n = 0.005$, (c) $F_n = 0.010$, (d) $F_n = 0.150$.

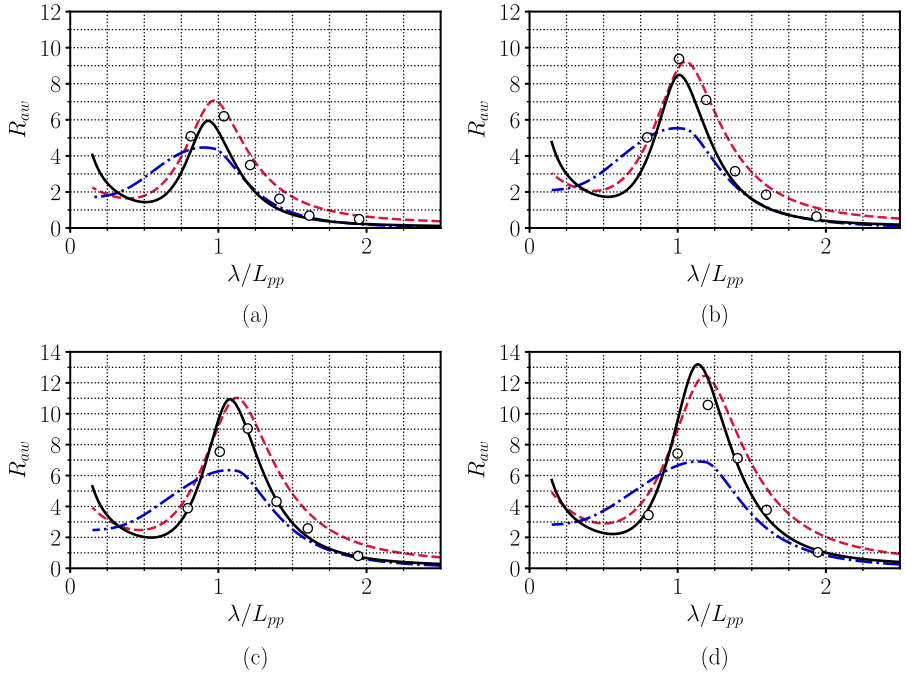

Fig. A.18. Added resistance of S.A Van Der Stel in the regular head wave, ○ experiment data, ——— CTH, -·-·- ITTC-STA2, - - - NTUA; estimated for (a) $F_n = 0.150$, (b) $F_n = 0.200$, (c) $F_n = 0.250$, (d) $F_n = 0.300$.

estimated by the proposed method is presented in Figs. 11 and 12 for the PCTC and the chemical tanker, respectively.

As illustrated in the two figures, the maximum speed loss for the case study PCTC at H_s = 3.1 m is about 2.4 kn, i.e., 14% involuntary speed reduction caused by the sea environments. For the chemical tanker, due to the highest encountered sea states of H_s = 7.1 m, the maximum speed loss is 4.9 kn, i.e., about 40% in voluntary speed reduction. It should be noted that under this very high sea state, the chemical tanker's power was already reduced by about 40% in comparison with her normal service conditions. If one compares the actual measured speeds and the estimated speeds, in general, the proposed models show consistently excellent prediction through all considered wave conditions for the case study PCTC, with a maximum difference of about 0.2 kn. The same agreement has also been observed for the chemical tanker in Fig. 12, while the validation cases start from $H_s \approx$ 1.4 m, to the harsh sea condition with significant wave height more than 7 m ($4.5 < H_s < 5.5$ m was skipped, because of too little measurements in that range). It should be noted that for the PCTC in Fig. 11, there is a consistently slight underestimation of added resistance due to waves, leading to higher estimated speeds V_{real}, while there is also an almost

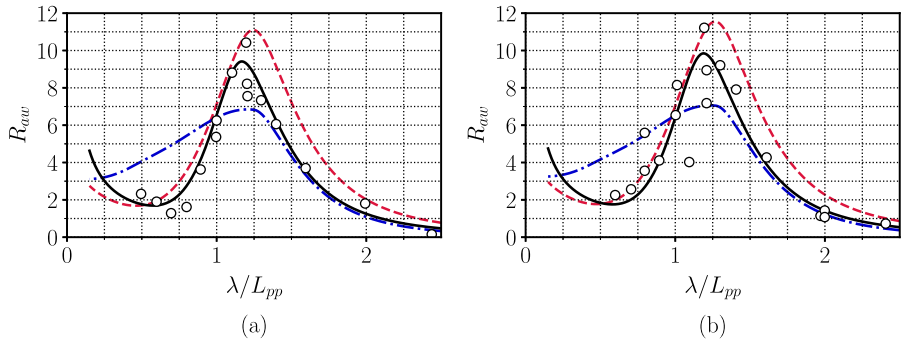

Fig. A.19. Added resistance of Series 60 model 4210 in the regular head wave, ○ experiment data, ——— CTH, -·-·- ITTC-STA2, - - - - NTUA; estimated for (a) $F_n = 0.266$, (b) $F_n = 0.283$.

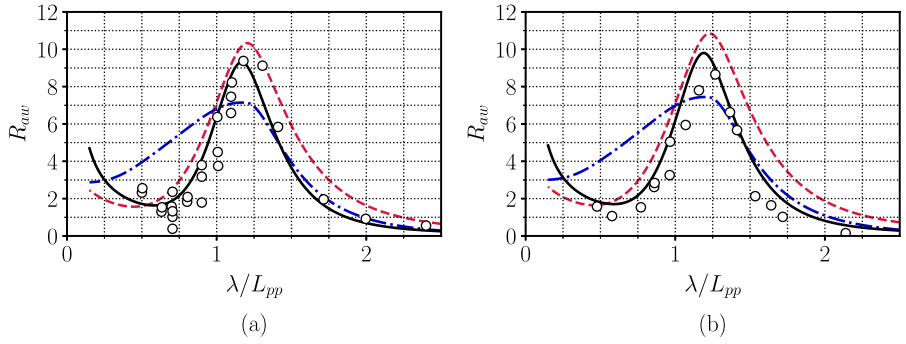

Fig. A.20. Added resistance of Series 60 model 4211 in the regular head wave, ○ experiment data, ——— CTH, -·-·- ITTC-STA2, - - - - NTUA; estimated for (a) $F_n = 0.237$, (b) $F_n = 0.254$.

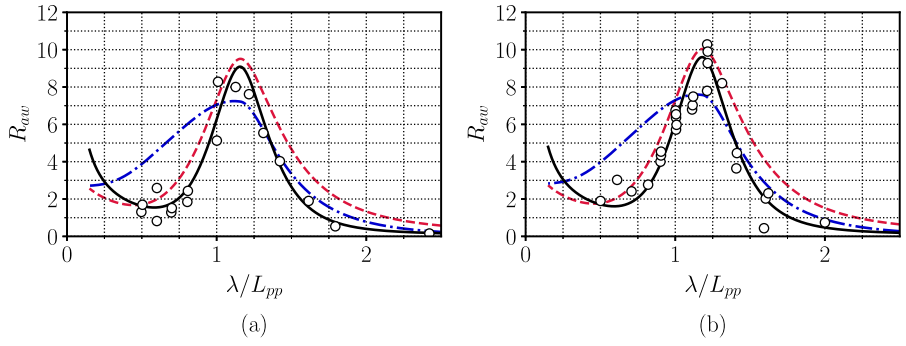

Fig. A.21. Added resistance of Series 60 model 4212 in the regular head wave, ○ experiment data, ——— CTH, -·-·- ITTC-STA2, - - - - NTUA; estimated for (a) $F_n = 0.207$, (b) $F_n = 0.222$.

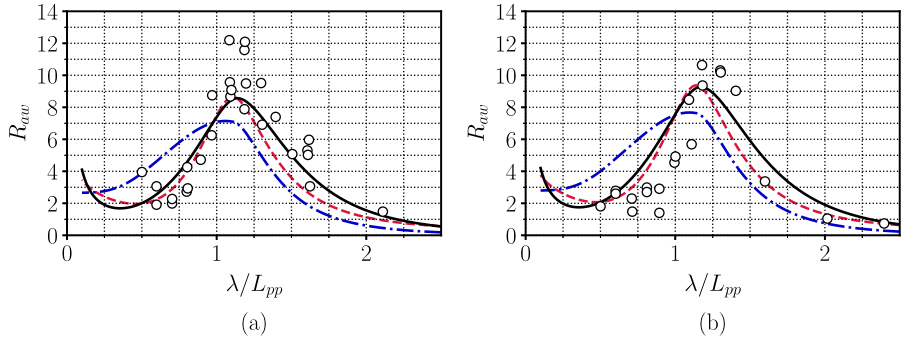

Fig. A.22. Added resistance of Series 60 model 4213 in the regular head wave, ○ experiment data, ——— CTH, -·-·- ITTC-STA2, - - - - NTUA; estimated for (a) $F_n = 0.177$, (b) $F_n = 0.195$.

consistently slight overestimation of added resistance for the chemical tanker. It might indicate that a ship type related correction factor should be considered in the proposed model for speed–power modeling. Since the difference is small, it will not be further investigated in this study.

6. Conclusions

This study proposed several improvements of current semi-empirical models for a ship's speed loss prediction when sailing in head sea conditions. It includes improved semi-empirical formulas for added

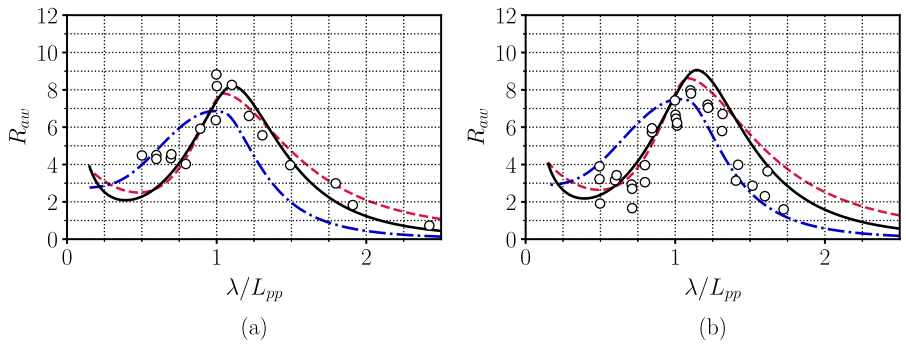

Fig. A.23. Added resistance of Series 60 model 4213 in the regular head wave, ○ experiment data, ——— CTH, -·-·- ITTC-STA2, - - - - NTUA; estimated for (a) $F_n = 0.147$, (b) $F_n = 0.165$.

resistance due to regular head waves through combining the further developed NMRI formulas (Fujii and Takahashi, 1975) for short waves (due to wave reflections), and the improved semi-empirical models from Jinkine and Ferdinande (1974) for long waves (due to wave motions). The improved semi-empirical models have been validated by an abundant of published experimental data in regular waves with sufficiently accurate approximations compared to the other two existed well-known approaches.

Furthermore, a special contribution in this study is to propose a wave height correction factor in the conventional formula by integrating wave spectrum with the semi-empirical added resistance in regular waves, to estimate the added resistance due to actual sea states (irregular waves described by wave spectrum). Two case study ships with full-scale measurements available are used to verify the proposed models for both the estimation of added resistance and speed loss prediction due to actual sea states. The measurements recorded, among others, ship speed, heading, position and shaft power, etc., while the reanalysis sea environmental data are applied to obtain the wave and wind conditions along with the measured sailing voyages. For the added resistance due to irregular head waves, the proposed models (with the wave height correction factor) using the JONSWAP wave spectrum give very good estimations in comparison with measured values for most of the investigated sea states. One exceptional case is for the extremely harsh sea state with H_s of more than 8.2 m. Even the extra added wave height factor still seriously underestimates the added resistance, because the extreme waves caused motions may affect the estimation of propulsion efficiencies in the analysis.

For the speed loss prediction under actual sailing sea environments, significant speed losses are observed from the two ships' measurement data, with a maximum 14% speed reduction at H_s of 3 meters for the PCTC, and 40% speed reduction for the chemical tanker at H_s of 7 meters in addition to certain voluntary speed reduction. The proposed models give excellent results in comparison with the measured results for both ships. The good agreement is obtained even for the high waves of H_s of more than 7 m. In general, the proposed semi-empirical models work well for the analysis of added resistance due to waves.

CRediT authorship contribution statement

Xiao Lang: Conceptualization, Methodology, Formal analysis, Writing - original draft, Investigation, Validation, Visualization, Software. **Wengang Mao:** Conceptualization, Supervision, Writing - review & editing, Formal analysis, Funding acquisition, Project administration.

Declaration of competing interest

The authors declare that they have no known competing financial interests or personal relationships that could have appeared to influence the work reported in this paper.

Acknowledgments

The authors acknowledge the financial support from the European Commission (Horizon 2020) project EcoSail (Grant Number 820593). We are also grateful to the support from the Swedish Foundation for International Cooperation in Research and Higher Education (CH2016-6673), National Natural Science Foundation of China (NSFC-51779202), and ship owners for providing model tests results and related full-scale measurements data.

Appendix. Experiment data validation results

See Figs. A.13–A.23.

References

Alexandersson, M., 2009. A study of methods to predict added resistance in waves. Royal Inst. Technol.

Boese, P., 1970. Eine einfache Methode zur Berechnung der Widerstandserhöhung eines Schiffes im Seegang. Schriftenreihe Schiffbau 258, 1–9.

Brandsæter, A., Vanem, E., 2018. Ship speed prediction based on full scale sensor measurements of shaft thrust and environmental conditions. Ocean Eng. 162, 316–330.

Carlton, J., 2012. Marine Propellers and Propulsion, fourth ed. Butterworth-Heinemann, Oxford, UK.

CMEMS, 2019. E.u. copernicus marine service information. URL: http://marine.copernicus.eu/. (Accessed 18 May 2019).

Copernicus, 2019. Copernicus Climate Change Service Climate Data Store (CDS), 2019, Copernicus Climate Change Service (C3S): ERA5: Fifth generation of ECMWF atmospheric reanalyses of the global climate. URL: https://cds.climate.copernicus.eu/cdsapp/home. (Accessed 16 May 2019.

de Jong, P., Katgert, M., Keuning, L., 2009. The development of a velocity prediction program for traditional Dutch sailing vessels of the type Skûtsje. In: Proceedings of the 20th International HISWA Symposium on Yacht Design and Yacht Construction.

DNV-GL, 2015. Energy Management Study 2015. Høvik, Norway.

Faltinsen, O.M., Minsaas, K.J., Liapis, N., Skjordal, S.O., 1980. Prediction of resistance and propulsion of a ship in a seaway. In: Proceedings of the 13th Symposium on Naval Hydrodynamics, pp. 505–529.

Fujii, H., Takahashi, T., 1975. Experimental study on the resistance increase of a large full ship in regular oblique waves. J. Soc. Naval Archit. Japan 1975 (137), 132–137.

Gerritsma, J., Beukelman, W., 1972. Analysis of the resistance increase in waves of a fast cargo ship. Int. Shipbuild. Prog. 19 (217), 285–293.

Grin, R., 2012. On the prediction of wave added resistance. In: Proceedings of 11Th International Marine Design Conference. IMDC, Glasgow, UK.

Guo, B., Steen, S., 2011. Evaluation of added resistance of kvlcc2 in short waves. J. Hydrodyn. 23 (6), 709–722.

Hasselmann, K., Barnett, T.P., Bouws, E., Carlson, H., Cartwright, D.E., Enke, K., Ewing, J.A., Gienapp, H., Hasselmann, D.E., Kruseman, P., Meerburg, A., Muller, P., Olbers, D.J., Richter, K., Sell, W., Walden, H., 1973. Measurements of wind-wave growth and swell decay during the joint north sea wave project (JONSWAP). Ergnzungsheft Dtsch. Hydrograph. Z. Reihe.

Hastie, T., Tibshirani, R., Friedman, J., 2009. The Elements of Statistical Learning, second ed. In: Springer Series in Statistics, Springer, New York, US.

Havelock, T., 1942. The drifting force on a ship among waves. London Edinburgh Dublin Phil. Mag. J. Sci. 33 (221), 467–475.

Holtrop, J., Mennen, G., 1982. An approximate power prediction method. Int. Shipbuild. Prog. 29 (335), 166–170.

IMO, 2009. Guidance for voluntary use of the ship energy efficiency operational indicator (EEOI), MEPC.1/Circ.684.
IMO, 2013. Interim guidelines for determining minimum propulsion power to maintain the manoeuvrability in adverse conditions, MEPC.232(65).
IMO, 2014. Guidelines on the method of calculation of the attained energy efficiency design index (EEDI) for new ships, MEPC.245(66).
ISO, 2015. Ships and marine technology - Guidelines for the assessment of speed and power performance by analysis of speed trial data, 15016.
ITTC, 2002. Resistance uncertainty analysis example for resistance test, Recommended procedures 7.5-02-02-02.
ITTC, 2012. Analysis of speed/power trial data, Recommended procedures and guidelines 7.5-04-01-01.2.
ITTC, 2017. Seakeeping experiments, Recommended procedures and guidelines 7.5-02-07-02.1.
ITTC, 2018. Calculation of the weather factor f_w for decrease of ship speed in wind and waves, Recommended Procedures and Guidelines 7.5-02-07-02.8.
Jinkine, V., Ferdinande, V., 1974. A method for predicting the added resistance of fast cargo ships in head waves. Int. Shipbuild. Prog. 21 (238), 149–167.
Kadomatsu, K., 1988. Study on the Required Minimum Output of Main Propulsion Engine Considering Maneuverability in Rough Sea (Ph.D. thesis). Yokohama National University, Japan.
Kuroda, M., Tsujimoto, M., Fujiwara, T., Ohmatsu, S., Takagi, K., 2008. Investigation on components of added resistance in short waves. J. Japan Soc. Nav. Archit. Ocean Eng. 8, 171–176.
Lewis, E.V., 1988. Principles of Naval Architecture, vol. 2. SNAME, second ed. The Society of Naval Architects and Marine Engineers, Jersey city, US.
Liu, S., Papanikolaou, A., 2016a. Fast approach to the estimation of the added resistance of ships in head waves. Ocean Eng. 112, 211–225.
Liu, S., Papanikolaou, A.D., Prediction of the added resistance of ships in oblique seas. In: Proceedings of the 26th International Ocean and Polar Engineering Conference.
Liu, S., Shang, B., Papanikolaou, A., Bolbot, V., 2016. Improved formula for estimating added resistance of ships in engineering applications. J. Mar. Sci. Appl. 15 (4), 442–451.
Lu, R., Turan, O., Boulougouris, E., Banks, C., Incecik, A., 2015. A semi-empirical ship operational performance prediction model for voyage optimization towards energy efficient shipping. Ocean Eng. 110, 18–28.
Maruo, H., 1957. The excess resistance of a ship in rough seas. Int. Shipbuild. Prog. 4 (35), 337–345.
Maruo, H., 1960. Wave resistance of a ship in regular head seas. Bull. Faculty Eng. Yokohama Natl. Univ. 9, 73–91.
Maruo, H., 1963. Resistance in waves, research on seakeeping qualities of ships in Japan. Soc. Nav. Archit. Japan 8, 67–102.
Moctar, O., Shigunov, V., Zorn, T., 2012. Duisburg test case: Post-panamax container ship for benchmarking. Ship Technol. Res. 59 (3), 50–64.
Moctar, O., Shigunov, V., Zorn, T., 2015. Duisburg test case: Post-panamax container ship for benchmarking. Ship Technol. Res. 50–64.
Pérez Arribas, F., 2007. Some methods to obtain the added resistance of a ship advancing in waves. Ocean Eng. 34 (7), 946–955.
Pierson, W.J., Moskowitz, L., 1964. A proposed spectral form for fully developed wind seas based on the similarity theory of S. A. Kitaigorodskii. J. Geophys. Res. 69 (24), 5181–5190.
Prpić-Oršić, J., Faltinsen, O.M., 2012. Estimation of ship speed loss and associated CO2 emissions in a seaway. Ocean Eng. 44, 1–10.
Sadat-Hosseini, H., Wu, P., Carrica, P.M., Kim, H., Toda, Y., Stern, F., 2013. CFD verification and validation of added resistance and motions of KVLCC2 with fixed and free surge in short and long head waves. Ocean Eng. 59, 240–273.
Salvesen, N., 1978. Added resistance of ships in waves. J. Hydronaut. 12 (1), 24–34.
Strom-Tejsen, J., Yeh, H., Moran, D., 1973. Added resistance in waves. Trans. Soc. Nav. Archit. Mar. Eng. 81, 109–143.
Takahashi, T., 1988. A practical prediction method of added resistance of a ship in waves and the direction of its application to hull form design. Trans. West-Japan Soc. Nav. Archit. 75 (75), 75–95.
Tsujimoto, M., Shibata, K., Kuroda, M., Takagi, K., 2008. A practical correction method for added resistance in waves. J. Japan Soc. Nav. Archit. Ocean Eng. 8, 177–184.
Ursell, F., Dean, W.R., 1947. The effect of a fixed vertical barrier on surface waves in deep water. Math. Proc. Camb. Phil. Soc. 43 (03), 374–382.
Valanto, P., Hong, Y., 2015. Experimental investigation on ship wave added resistance in regular dead, oblique, beam, and following waves. In: Proceedings of the 25th International Society of Offshore and Polar Engineers.
Wang, H., Mao, W., Eriksson, L., 2019. A three-dimensional Dijkstra's algorithm for multi-objective ship voyage optimization. Ocean Eng. 185, 106131.